Journal of Computational and Applied Mathematics 270 (2014) 471–483

Contents lists available at ScienceDirect

Journal of Computational and Applied Mathematics

journal homepage: www.elsevier.com/locate/cam

A hybrid level set/front tracking approach for finite element simulations of two-phase flows

Steffen Basting *, Martin Weismann

Department of Mathematics, Friedrich-Alexander-University Erlangen-Nuremberg, Cauerstr. 11, 91058 Erlangen, Germany

ARTICLE INFO

Article history:
Received 24 September 2013
Received in revised form 3 December 2013

Keywords:
Level set method
Front tracking
Mesh optimization
Arbitrary Lagrangian–Eulerian formulation
Two-phase flow

ABSTRACT

In this paper we give details on the numerical realization of a new finite element method for the simulation of two-phase flows which was recently introduced in Basting and Weismann (2013). The main ingredient is a hybrid representation of the interface between the fluid phases: An implicit description of the interface is given by a level set function and an explicit representation is obtained from aligning edges of the computational mesh to the implicitly described interface. This step is done by a black-box optimization based mesh smoothing approach which does not change the topology of the mesh while guaranteeing optimal mesh quality. Furthermore, we make use of quadratic isoparametric elements to increase the approximation quality of the discrete interface.

Due to the alignment, discontinuities of the solution variables (pressure) can be captured accurately, while a variational treatment of the curvature allows for a precise approximation of surface tension. We present our time discretization scheme for the coupled Navier–Stokes/level set equations, and discuss our space discretization based on the so called subspace projection method (SPM) to account for discontinuities across the interface.

We present two numerical examples for which reference solutions exist. We consider the oscillation of a single droplet and provide our results for an established two-phase flow benchmark problem.

1. Introduction

When it comes to numerical methods for flow problems with free interfaces, the representation of the interface is a key issue. Consequently, over the years, many approaches have been proposed. Most of these approaches may be classified as either *interface capturing* or *interface tracking* methods.

In *interface capturing* methods, the interface is represented implicitly by an additional function, for instance as a distance function in the level set method [1,2] or by means of a volume fraction in VOF methods [3]. Commonly, these methods are defined on structured meshes. Due to the implicit representation of the interface, these methods are especially powerful when strong deformations of the interface occur. However, if interface forces such as surface tension play an essential role, special care has to be taken with regard to its discretization. Furthermore, since the computational mesh is in general not aligned with the interface, solution properties such as discontinuities of the pressure across the interface are difficult to capture.

On the other hand, in *interface tracking* methods, the interface is discretized explicitly. This can be achieved by additional markers which are transported by the flow field, or by a separate interface mesh. A special class of interface tracking

* Corresponding author. Tel.: +49 9131 8567228.
E-mail addresses: basting@math.fau.de (S. Basting), weismann@math.fau.de (M. Weismann).

0377-0427/$ – see front matter © 2013 Elsevier B.V. All rights reserved.
http://dx.doi.org/10.1016/j.cam.2013.12.014

methods is obtained from aligning the computational mesh with the discrete interface. Usually, in these *aligned interface methods*, equations are formulated in arbitrary Lagrangian–Eulerian (ALE) coordinates [4] which allows for the movement of the computational mesh with the interface. In this case, the aforementioned problems of surface tension evaluation and representation of discontinuities of the pressure can be treated very easily: due to the alignment, a discrete representation of the interface is always at hand in terms of edges of the computational mesh, and finite element spaces taking discontinuities into account may be realized quite easily. However, the movement may lead to degeneration of the computational mesh. Although techniques such as remeshing or special extension operators allow to deal with more complex situations (see for instance [5,6] for numerical studies on different mesh moving strategies for problems with large deformations), these methods are usually applied when deformations of the interface can be expected to be "mild".

A hybrid approach which aims at combining interface capturing and interface tracking methods to achieve enhanced geometrical flexibility while retaining the benefits of aligned mesh methods was introduced in [7] and applied to particulate flows in [8]. The main idea is to use a level set representation of the interface while aligning the computational mesh with the zero level set in each time step. This is achieved in an automatic way by a black-box mesh optimization approach. The interface is always approximated by certain edges of the mesh (which are not specified a priori as in "classical" aligned interface methods). In this paper, we review this approach and give details on the time and space discretization of the method presented in [7]: We discuss a splitting of the coupled Navier–Stokes/level set equations in time, time discretization of the resulting subproblems and show how a finite element space which is able to capture the discontinuity of the pressure across the interface can be realized using a discrete projection (the subspace projection method), which was introduced in [9–11].

We present two numerical examples to demonstrate the benefits but also the limitations of our proposed approach.

2. Mathematical model

We consider the behavior of two immiscible, incompressible Newtonian fluids modeled by the incompressible Navier–Stokes equations. More precisely, we assume to have one time independent domain $\Omega \subset \mathbb{R}^2$ occupied by two time dependent fluid domains $\Omega_1(t)$, $\Omega_2(t)$ which are separated by a sharp interface $\Gamma(t)$, i.e. $\bar{\Omega} = \bar{\Omega}_1(t) \cup \bar{\Omega}_2(t)$, $\Omega_1(t) \cap \Omega_2(t) = \emptyset$ and $\Gamma(t) = \bar{\Omega}_1(t) \cap \bar{\Omega}_2(t)$ for time instants $t \in [0, T]$. In each domain $\Omega_i(t)$, we require the fluid to have constant density ρ_i and viscosity μ_i.

The governing equations in the bulk read in dimensionless form

$$\left.\begin{aligned} &\Lambda_i \left(\partial_t \mathbf{u} + (\mathbf{u} \cdot \nabla)\, \mathbf{u}\right) - \nabla \cdot \boldsymbol{\sigma}_i = \Lambda_i \mathbf{f} \\ &\nabla \cdot \mathbf{u} = 0 \end{aligned}\right\} \quad \text{in } \Omega_i(t), \tag{1}$$
$$\mathbf{u} = 0 \quad \text{on } \partial\Omega,$$

where $\mathbf{u}$ denotes velocity, p pressure, $\mathbf{f}$ denotes the vector of external forces and

$$\Lambda_i = \frac{\rho_i}{\rho_c}, \qquad \mathrm{Re}_i = \frac{\rho_i U L}{\mu_i}, \qquad \boldsymbol{\sigma}_i = \frac{1}{\mathrm{Re}_i}\left(\nabla \mathbf{u} + (\nabla \mathbf{u})^T\right) - p\mathbb{1}$$

denote density ratio (with reference density ρ_c), Reynolds number and stress tensor for each domain. U denotes a characteristic velocity and L a characteristic length scale.

If we denote the constant surface tension coefficient by σ and the curvature of Γ by κ, the capillary boundary condition on Γ is given by

$$[\![\boldsymbol{\sigma}(\mathbf{u}, p)]\!] = \frac{1}{\mathrm{We}} \kappa \mathbf{n} \quad \text{on } \Gamma(t) \tag{2}$$

with Weber number $\mathrm{We} = \frac{\rho_c U^2 L}{\sigma}$. The movement of the interface Γ is prescribed by the kinematic boundary condition

$$V_\Gamma = \mathbf{u} \cdot \mathbf{n} \quad \text{on } \Gamma(t). \tag{3}$$

In this paper, we make use of the arbitrary Lagrangian–Eulerian (ALE) formulation [4] of the mathematical model to follow the movement of the fluid interface. To this end, we consider a fixed reference domain $\hat{\Omega} \subset \mathbb{R}^2$ whose boundary coincides with the boundary of Ω, i.e. $\partial\hat{\Omega} = \partial\Omega(t)\ \forall t$. We assume to have a smooth mapping

$$\begin{aligned} &\boldsymbol{\xi} : [0, T] \times \hat{\Omega} \to \mathbb{R}^2, \\ &\boldsymbol{\xi}(t, \hat{\Omega}) = \Omega(t) \quad \text{for all } t \in [0, T]. \end{aligned}$$

For each time instant $t \in [0, T]$, we assume $\boldsymbol{\xi}$ to be a homeomorphism. The velocity of the domain $\mathbf{w}$ is defined as

$$\begin{aligned} &\mathbf{w}(t, \cdot) : \Omega(t) \to \mathbb{R}^2, \\ &\mathbf{w}(t, \cdot) = \partial_t \boldsymbol{\xi}(t, \boldsymbol{\xi}(t, \cdot)^{-1}). \end{aligned} \tag{4}$$

For any sufficiently smooth function $F : [0, T] \times \mathbb{R}^2 \to \mathbb{R}$ we may define the ALE time derivative of F as

$$\hat{\partial}_t F(t, \mathbf{x}) := \partial_t F(t, \boldsymbol{\xi}(t, \hat{\mathbf{x}})) = \partial_t F(t, \mathbf{x}) + \mathbf{w}(t, \mathbf{x}) \cdot \nabla F(t, \mathbf{x}) \tag{5}$$

for $\mathbf{x} = \boldsymbol{\xi}(t, \hat{\mathbf{x}})$, $\hat{\mathbf{x}} \in \hat{\Omega}$.

Replacing the time derivative in (1) with the ALE time derivative from relation (5), we arrive at the following system:

$$\left.\begin{aligned} &\Lambda_i\left(\hat{\partial}_t\mathbf{u} + ((\mathbf{u}-\mathbf{w})\cdot\nabla)\,\mathbf{u}\right) - \nabla\cdot\boldsymbol{\sigma}_i = \Lambda_i\mathbf{f} \\ &\nabla\cdot\mathbf{u} = 0 \end{aligned}\right\} \quad \text{in } \Omega_i(t) \tag{6}$$
$$\mathbf{u} = 0 \quad \text{on } \partial\Omega.$$

Remark 1. So far, we have not made any requirements on the ALE mapping $\boldsymbol{\xi}$. In classical ALE models, the mapping is usually chosen in such a way that a certain reference interface $\hat{\Gamma} \subset \hat{\Omega}$ (in a discrete sense, for instance, given by fixed edges of the triangulation of the reference domain $\hat{\Omega}$) matches the time dependent interface Γ, i.e.

$$\boldsymbol{\xi}(t, \hat{\Gamma}) = \Gamma(t) \quad \text{for all } t \in [0, T].$$

In the proposed approach, we do not prescribe such a fixed reference configuration but construct a mapping which may lead to different parametrizations of $\Gamma(t)$ in time.

In order to track the interface Γ over time, we assume that both phases Ω_i and the interface Γ may be written in terms of a continuous level set function $\phi : [0, T] \times \Omega \to \mathbb{R}$:

$$\begin{aligned} \Omega_{1/2}(t) &= \{\mathbf{x} \in \Omega : \phi(t, \mathbf{x}) \gtrless 0\}, \\ \Gamma(t) &= \{\mathbf{x} \in \Omega : \phi(t, \mathbf{x}) = 0\}. \end{aligned} \tag{7}$$

The evolution of the interface Γ is then given by the transport equation for the level set function ϕ,

$$\hat{\partial}_t\phi + ((\mathbf{u}-\mathbf{w})\cdot\nabla)\,\phi = 0 \quad \text{for all } \mathbf{x} \in \Omega,\ t \in [0, T] \tag{8}$$

and appropriate initial conditions such that $\Gamma(0) = \{\mathbf{x} \in \Omega : \phi(0, \mathbf{x}) = 0\}$.

3. Geometry representation: level set aligned, optimal triangulations

In this section, we briefly revisit the main building block of our hybrid approach, a detailed description was already presented in [7,12]. The method is based on two ingredients:

- A variational mesh optimization technique which produces triangulations of "optimal" quality by modifying nodal coordinates and
- an additional constraint on the mesh optimization problem to enforce the alignment of Γ and edges of the resulting triangulation.

In the following subsections, we proceed with a brief outline of our mesh alignment method.

3.1. Optimal triangulations

Our approach to obtaining level set aligned, optimal triangulations is based on a variational mesh optimization technique for simplicial triangulations which was introduced and analyzed by M. Rumpf [13]. Given an initial triangulation $\mathcal{T}$ of the domain Ω, the idea is to find an "optimal" triangulation $\mathcal{T}^* = \varphi^*(\mathcal{T})$ resulting from an optimal mesh deformation $\varphi^* \in D$. These deformations are assumed to be piecewise affine, orientation preserving and globally continuous i.e.

$$D = \left\{\varphi \in \mathcal{C}^0(\Omega) : \nabla\varphi_{|T} \in \mathrm{GL}(2),\ \det(\nabla\varphi_{|T}) > 0\ \forall T \in \mathcal{T}\right\},$$

where $\mathrm{GL}(n) = \{A \in \mathbb{R}^{n\times n} : \det(A) \neq 0\}$ denotes the general linear group over $\mathbb{R}^n$. An optimal deformation $\varphi^* \in D$ can be found as the minimizer of certain functionals $\mathcal{F}$:

$$\mathcal{F}(\varphi^*) = \min_{\varphi\in D} \mathcal{F}(\varphi). \tag{9}$$

We assume that the functionals in (9) can be represented by a sum of weighted, element-wise contributions,

$$\mathcal{F}(\varphi) = \sum_{T\in\mathcal{T}} \mu_T F_T(\varphi) \tag{10}$$

where $\mu_T > 0$, $\sum_T \mu_T = 1$ denotes a positive weight and F_T the contribution of the deformation φ restricted to T. Assuming translational invariance, isotropy and frame indifference of the functionals it can be shown (see [13]) that the local contribution F_T may be expressed in terms of the invariants of the linear reference mapping $R_T : h(T)T^* \to T$, where T^* denotes the normalized equilateral simplex and $h(T)$ denotes the desired edge length for T. In two dimensions, F_T takes the form

$$F_T = F(\|\nabla R_T(\varphi)\|^2, \det(\nabla R_T(\varphi))) =: F(a, d). \tag{11}$$

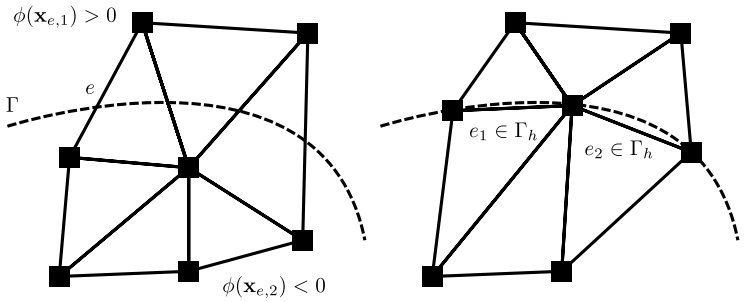

Fig. 1. A triangulation *not* aligned to Γ (left) and aligned triangulation (right).

The optimally deformed simplex $h(T)T^*$ is obtained if $\varphi^*_{|T} = \mathrm{Id}$, i.e. if

$$F_T(\varphi^*) = \min_{\varphi} F_T(\varphi) = F_T(\mathrm{Id}) = F(\|\mathrm{Id}\|^2, \det(\mathrm{Id})) = F(2, 1).$$

In order to rule out deformations with vanishing determinant, we also assume that $\lim_{\det(\nabla R_T(\varphi))\to 0} F_T(\varphi) = \infty$. A typical example of the local function F_T is given by

$$F(a, d) = (a - 2)^2 + d + \frac{1}{d}. \tag{12}$$

Note that the quantity $a = \|\nabla R_T(\varphi)\|^2$ measures the change of edge lengths with respect to the reference element and $d = \det(\nabla R_T(\varphi))$ measures the change in volume. Let us close this section by briefly summarizing the properties and benefits of the variational mesh smoothing approach (see also [13,7,12]):

- Minimizing (10) yields triangulations $\mathcal{T}^*$ which are optimal in the sense of the local measure (12).
- These triangulations can be shown to be non-degenerate (no self-intersection of elements occurs).
- The element-wise representation of $\mathcal{F}$ provides built-in, local mesh quality control.
- r-adaptivity can be easily achieved by prescribing desired edge lengths for each mesh element.
- The functional $\mathcal{F}$ is highly non-linear, non-convex and global minimizers may be non-unique.

3.2. Level set alignment

We are now interested in adjusting the position of the nodes in such a way that edges of the triangulation approximate the interface Γ. This can be achieved by explicitly shifting certain nodes onto Γ (see for instance [14] for such an approach). However, in our approach we would like to circumvent the combinatorial work required for such a method. To this end, we make a key observation regarding the alignment of edges of the triangulation with the interface Γ: Consider the situation depicted in Fig. 1 and let e be an arbitrary edge of the triangulation $\mathcal{T}$. By $\mathbf{x}_{e,1}$ and $\mathbf{x}_{e,2}$ we denote the nodes adjacent to edge e. Due to continuity of ϕ and assumption (7), we conclude that

$$\phi(\mathbf{x}_{e,1})\phi(\mathbf{x}_{e,2}) < 0 \tag{13}$$

if and only if e is intersected by Γ (provided that the mesh size h is sufficiently small to resolve the shape of Γ). We therefore define the triangulation to be *linearly aligned* with Γ if

$$\phi(\mathbf{x}_{e,1})\phi(\mathbf{x}_{e,2}) \geq 0 \quad \text{for all } e \in \mathcal{T}. \tag{14}$$

If we employ the mesh optimization procedure introduced in the last section, we may rule out non aligned triangulations by introducing the single scalar constraint

$$c : D \to \mathbb{R}_0^+,$$
$$c(\varphi) = \sum_{e\in\varphi(\mathcal{T})} \mathcal{H}(\phi(\mathbf{x}_{e,1})\phi(\mathbf{x}_{e,2})) \quad \text{where}$$
$$\mathcal{H}(z) := \begin{cases} > 0 & \text{if } z < 0, \\ = 0 & \text{otherwise.} \end{cases}$$

Restricting the set of admissible deformations to deformations for which $c(\varphi) = 0$, a linearly aligned triangulation of optimal quality is obtained from the constrained optimization problem

$$\min_{\varphi\in D} \mathcal{F}(\varphi) \quad \text{such that } c(\varphi) = 0. \tag{15}$$

Details on the numerical realization of this problem can be found in [7,12].

A linearly aligned triangulation is sketched in Fig. 1. Given such an aligned triangulation, we may define a linear approximation to the interface Γ as

$$\Gamma_h(\mathcal{T}) := \left\{ e \in \mathcal{T} : \phi(\mathbf{x}_{e,i}) = 0 \text{ for } i = 1, 2 \right\}. \tag{16}$$

In order to increase the approximation quality of Γ_h, we also consider piecewise quadratic approximations to Γ. To this end, we first construct a piecewise linear representation Γ_h as described above. If we introduce the reference simplex $\hat{K} = \{\hat{\mathbf{x}} \in \mathbb{R}^2 : \sum_{i=1}^{2} \hat{x}^{(i)} \leq 1, \hat{x}^{(i)} \geq 0\}$ and the quadratic isoparametric mapping $G_K : \hat{K} \to K$ by

$$G_K(\hat{\mathbf{x}}) = \sum_{i=1}^{6} \mathbf{x}_i \varphi_i(\hat{\mathbf{x}}),$$

where φ_i, $i = 1, \ldots, 6$ denote the quadratic Lagrange basis functions, each edge $e \in \Gamma_h$ may be expressed as

$$e = G_K(\hat{e}) = \left\{ \sum_{i=1}^{2} \mathbf{x}_{e,i} \varphi_i(\hat{\mathbf{x}}) + \mathbf{x}_m \varphi_3(\hat{\mathbf{x}}) \text{ for } \hat{\mathbf{x}} \in \hat{e} := [0, 1] \times \{0\} \right\}.$$

The quadratic node $\mathbf{x}_m$ is then shifted onto the zero level set of ϕ, resulting in a quadratic approximation to Γ. Details on the numerical realization together with an evaluation of mesh and approximation quality and computational costs can be found in [7,8,12].

4. Time and space discretization

In this section, we present our numerical method to solving Eqs. (6) and (8). The numerical treatment of this system is very challenging due to the strong coupling and appearance of strong nonlinearities (in the Navier–Stokes equations, curvature of the interface and especially due to the time dependency of the ALE parametrization $\boldsymbol{\xi}$).

4.1. Decoupling of the problems

For an efficient solution strategy, we first decouple the problem into a series of "simpler" subproblems. To this end, we discretize the time interval $[0, T]$ with time instants $t_k = \tau k$ for a fixed time step size $\tau > 0$ and write $\Omega^k := \Omega(t_k)$, $\mathbf{u}^k(\cdot) := \mathbf{u}(t_k, \cdot)$, $p^k(\cdot) := p(t_k, \cdot)$. The solution strategy is based on the following time stepping procedure:

For each time instant t_k,

1. Solve for the flow variables $\mathbf{u}^{k+1}$, p^{k+1} on Ω^k.
2. Using $\mathbf{u}^{k+1}$ solve the transport equation for ϕ^{k+1} on Ω^k.
3. Obtain new partitioning of Ω into Ω_i^{k+1} and corresponding discrete interface Γ_h^{k+1} by the mesh optimization procedure from Section 3. Update the mesh velocity according to $\mathbf{w}^{k+1} = (\mathbf{x}^{k+1} - \mathbf{x}^k)/\tau$.

In what follows, we will discuss the first two steps of the time stepping procedure in detail.

4.2. Weak formulation

We proceed by deriving a weak formulation and discretizing in time (Rothe's method) the problems arising in the first two steps of the time-stepping procedure. To this end, we introduce the function spaces

$$\mathbf{X}_0 = \left(H_0^1(\Omega)\right)^2, \qquad W_{\mathbf{u}} = \left\{\phi \in L^2(\Omega) : \mathbf{u} \cdot \nabla\phi \in L^2(\Omega)\right\} \quad \text{and} \quad Y = L^2(\Omega).$$

Multiplying (6), (8) by suitable test functions $\mathbf{v} \in \mathbf{X}_0$, $q \in Y$ and $v \in Y$ and integrating over $\Omega_i(t)$ we obtain:

For $i = 1, 2$ and almost all $t \in [0, T]$ find $\mathbf{u}(t, \cdot) \in X_0$, $p(t, \cdot) \in Y$ and $\phi(t, \cdot) \in W_{\mathbf{u}-\mathbf{w}}$ such that

$$\begin{aligned}
&\int_{\Omega_i(t)} \Lambda_i \hat{\partial}_t \mathbf{u} + \Lambda_i((\mathbf{u} - \mathbf{w}) \cdot \nabla)\mathbf{u} \cdot \mathbf{v} - \frac{1}{\mathrm{Re}_i} \Delta\mathbf{u} \cdot \mathbf{v} + \nabla p \cdot \mathbf{v} = \int_{\Omega_i(t)} \Lambda_i \mathbf{f} \cdot \mathbf{v}, \\
&\int_{\Omega_i(t)} \nabla \cdot \mathbf{u} q = 0, \\
&\int_{\Omega} \hat{\partial}_t \phi v + (\mathbf{u} - \mathbf{w}) \cdot \nabla\phi v = 0.
\end{aligned} \tag{17}$$

The capillary boundary condition (2) can be integrated in the weak form by integrating by parts $-\int_{\Omega} (\nabla \cdot \boldsymbol{\sigma}_i) \cdot \mathbf{v}$ which yields

$$-\int_{\Omega} (\nabla \cdot \boldsymbol{\sigma}_i) \cdot \mathbf{v} = \sum_{i=1}^{2} \frac{1}{2\mathrm{Re}_i} \int_{\Omega_i(t)} \mathbf{D}(\mathbf{u}) : \mathbf{D}(\mathbf{v}) - \int_{\Omega} p \nabla \cdot \mathbf{v} - \frac{1}{\mathrm{We}} \int_{\Gamma(t)} \kappa \mathbf{n} \cdot \mathbf{v}.$$

The last term in the previous equation can then be treated using the Laplace–Beltrami characterization of the curvature proposed by Dziuk in [15],

$$-\int_{\Gamma(t)} \kappa \mathbf{n}\cdot\mathbf{v} = -\int_{\Gamma(t)} (\underline{\Delta}\mathbf{x})\cdot\mathbf{v} = \int_{\Gamma(t)} \underline{\nabla}\mathbf{x} : \underline{\nabla}\mathbf{v},$$

where $\underline{\Delta}$ denotes the Laplace–Beltrami operator and $\underline{\nabla}$ denotes the tangential gradient $\underline{\nabla} = (\mathrm{Id} - \mathbf{n}\mathbf{n}^T)\nabla$.

We now introduce the following linear forms on Ω and Γ:

$$m(\Omega;\mathbf{u},\mathbf{v}) = \sum_{i=1}^{2}\int_{\Omega_i} \Lambda_i \mathbf{u}\cdot\mathbf{v}, \tag{18a}$$

$$a(\Omega;\mathbf{u},\mathbf{v}) = \sum_{i=1}^{2}\int_{\Omega_i} \frac{1}{2\mathrm{Re}_i}\mathbf{D}(\mathbf{u}) : \mathbf{D}(\mathbf{v}), \tag{18b}$$

$$c(\Omega;\mathbf{u};\mathbf{v},\mathbf{w}) = \sum_{i=1}^{2}\int_{\Omega_i} \Lambda_i\,(\mathbf{u}\cdot\nabla)\,\mathbf{v}\cdot\mathbf{w}, \tag{18c}$$

$$b(\Omega;p,\mathbf{v}) = -\int_{\Omega} p\nabla\cdot\mathbf{v}, \tag{18d}$$

$$f(\Omega;\mathbf{v}) = \sum_{i=1}^{2}\int_{\Omega_i} \Lambda_i \mathbf{f}\cdot\mathbf{v}, \tag{18e}$$

$$e(\Gamma;\mathbf{v}) = \frac{1}{\mathrm{We}}\int_{\Gamma} \underline{\nabla}\mathbf{x} : \underline{\nabla}\mathbf{v}. \tag{18f}$$

Using these linear forms (17) can be written as

For almost all $t \in [0,T]$ *find* $\mathbf{u}(t,\cdot)\in X_0$, $p(t,\cdot)\in Y$ *and* $\phi(t,\cdot)\in W_{\mathbf{u}-\mathbf{w}}$ *such that*

$$m(\Omega(t);\hat{\partial}_t\mathbf{u},\mathbf{v}) + c(\Omega(t);\mathbf{u}-\mathbf{w};\mathbf{u},\mathbf{v}) + a(\Omega(t);\mathbf{u},\mathbf{v}) + b(\Omega(t);p,\mathbf{v}) = f(\Omega(t);\mathbf{v}) - e(\Gamma(t);\mathbf{v}) \quad \forall \mathbf{v}\in\mathbf{X}_0, \tag{19a}$$

$$b(\Omega(t);q,\mathbf{u}) = 0 \quad \forall q\in Y, \tag{19b}$$

$$(\hat{\partial}_t\phi, v) + ((\mathbf{u}-\mathbf{w})\cdot\nabla\phi, v) = 0 \quad \forall v\in L^2(\Omega) \tag{19c}$$

with initial data

$$\mathbf{u}(0,\cdot) = \mathbf{u}_0(\cdot) \quad \text{and} \quad \phi(0,\cdot) = \phi_0(\cdot) \quad \text{in } \Omega.$$

4.3. Time discretization

We first comment on the time discretization of the Navier–Stokes equations (19a) and (19b). A critical part is the handling of the curvature term $e(\Gamma;\mathbf{v})$. An explicit treatment of this term will lead to a CFL condition of $\tau \le C\sqrt{\mathrm{We}}\,h^{3/2}$ [16] and in order to avoid the computational effort which comes with a fully implicit scheme, we use a semi-implicit treatment: the integration domain is associated with the current time instant t_k while the evaluation of the curvature is associated with the next time step t_{k+1}. To this end, we consider a discrete version of the kinematic boundary condition (3):

$$\mathbf{x}^{k+1} = \mathbf{x}^k + \tau\mathbf{u}^{k+1}$$

and define the bilinear form

$$d(\Gamma;\mathbf{u},\mathbf{v}) = \int_{\Gamma} \underline{\nabla}\mathbf{u} : \underline{\nabla}\mathbf{v}. \tag{20}$$

Using the semi-implicit discretization of the curvature term $e(\Gamma;\cdot)$,

$$e(\Gamma^{k+1};\mathbf{v}) \approx e(\Gamma^k;\mathbf{v}) + \tau d(\Gamma^k;\mathbf{u}^{k+1},\mathbf{v}),$$

unconditional stability for the resulting discretization was proved in [17].

For the discretization of the Navier–Stokes equations, we use the fractional step theta-scheme in an operator splitting variant proposed in [18]. We also refer to [19,20] for further information on time discretization in the ALE frame. Using the bilinear forms (19) and the semi-implicit treatment of the curvature term in (21), the modified fractional step theta-scheme reads (see also [21] for a single-phase version with free capillary boundary):

Let $(\Theta,\Theta',\alpha,\beta) = (1-\frac{1}{2}\sqrt{2},\frac{1}{2}\sqrt{2},2-\sqrt{2},\sqrt{2}-1)$

Quasi-Stokes substep (QS1): *Find* $\left(\mathbf{u}^{k+\Theta}, p^{k+\Theta}\right) \in \mathbf{X}_0 \times Y$ *such that*

$$m\left(\Omega^k; \frac{\mathbf{u}^{k+\Theta} - \mathbf{u}^k}{\Theta\tau}, \mathbf{v}\right) + \alpha a(\Omega^k; \mathbf{u}^{k+\Theta}, \mathbf{v}) + \tau d(\Omega^k; \mathbf{u}^{k+\Theta}, \mathbf{v}) + b(\Omega^k; p^{k+\Theta}, \mathbf{v})$$
$$= f(\Omega^k; \mathbf{v}) - c(\Omega^k; \mathbf{u}^k - \mathbf{w}^k; \mathbf{u}^k, \mathbf{v}) - \beta a(\Omega^k; \mathbf{u}^k, \mathbf{v}) - e(\Gamma^k; \mathbf{v}), \tag{21a}$$
$$b(\Omega^k; q, \mathbf{u}^{k+\Theta}) = 0 \tag{21b}$$

for all $(\mathbf{v}, q) \in (\mathbf{X}_0, Y)$.

Nonlinear substep (NL): *Find* $\mathbf{u}^{k+\Theta'} \in \mathbf{X}_0$ *such that*

$$m\left(\Omega^k; \frac{\mathbf{u}^{k+\Theta'} - \mathbf{u}^{k+\Theta}}{(1-2\Theta)\tau}, \mathbf{v}\right) + \beta a(\Omega^k; \mathbf{u}^{k+\Theta'}, \mathbf{v}) + c(\Omega^k; \mathbf{u}^{k+\Theta'} - \mathbf{w}^k; \mathbf{u}^{k+\Theta'}, \mathbf{v}) + \tau d(\Omega^k; \mathbf{u}^{k+\Theta'}, \mathbf{v})$$
$$= f(\Omega^k; \mathbf{v}) - \alpha a(\Omega^k; \mathbf{u}^{k+\Theta}, \mathbf{v}) - b(\Omega^k; p^{k+\Theta}, \mathbf{v}) - e(\Gamma^k; \mathbf{v}) \tag{22}$$

for all $\mathbf{v} \in \mathbf{X}_0$.

Quasi-Stokes substep (QS2): *Find* $\left(\mathbf{u}^{k+1}, p^{k+1}\right) \in \mathbf{X}_0 \times Y$ *such that*

$$m\left(\Omega^k; \frac{\mathbf{u}^{k+1} - \mathbf{u}^{k+\Theta'}}{\Theta\tau}, \mathbf{v}\right) + \alpha a(\Omega^k; \mathbf{u}^{k+1}, \mathbf{v}) + \tau d(\Omega^k; \mathbf{u}^{k+1}, \mathbf{v}) + b(\Omega^k; p^{k+1}, \mathbf{v})$$
$$= f(\Omega^k; \mathbf{v}) - c(\Omega^k; \mathbf{u}^{k+\Theta'} - \mathbf{w}^k; \mathbf{u}^{k+\Theta'}, \mathbf{v}) - \beta a(\Omega^k; \mathbf{u}^{k+\Theta'}, \mathbf{v}) - e(\Gamma^k; \mathbf{v}), \tag{23a}$$
$$b(\Omega^k; q, \mathbf{u}^{k+1}) = 0 \tag{23b}$$

for all $(\mathbf{v}, q) \in (\mathbf{X}_0, Y)$.

Note that the fractional step theta-scheme decouples two main difficulties of the Navier–Stokes equations: The nonlinear term in the momentum balance is treated in the second substep **(NL)** while the incompressibility condition is treated in the first and last substeps **(QS1)** and **(QS2)**. Substeps **(QS1)** and **(QS2)** can be expressed formally using a bilinear form

$$s : (\mathbf{X}_0 \times Y) \times (\mathbf{X}_0 \times Y) \to \mathbb{R}$$

and linear form

$$g : \mathbf{X}_0 \times Y \to \mathbb{R}.$$

Using these forms, the generic discretized problem reads: *Find* $(\mathbf{u}, p) \in \mathbf{X}_0 \times Y$ *such that*

$$s((\mathbf{u}, p), (\mathbf{v}, q)) = g(\mathbf{v}, q) \quad \text{for all } (\mathbf{v}, q) \in \mathbf{X}_0 \times Y. \tag{24}$$

We proceed with commenting on space discretization and postpone the treatment of the level set equation (19c) until Section 4.5.

4.4. Space discretization

In order to derive a stable discretization for Eqs. (21), (23) we employ the LBB-stable quadratic Taylor–Hood finite element defined on isoparametric elements. However, in view of the capillary boundary condition (2), the pressure space should be able to capture discontinuities across the interface Γ. This aspect, together with an accurate treatment of the curvature, is essential to avoid instabilities which may arise due to spurious velocities (see for instance [22–24]). In order to deal with the discontinuity of the pressure, for each time instant t_k we first introduce the *decoupled* Taylor–Hood spaces

$$\tilde{X}_h^k = \left\{ v_h \in H^1(\Omega_h^k) : v_{h|K} \circ G_K^2 \in P_2(\hat{K}),\, v_{h|\Omega_{h,i}^k} \in C^0(\Omega_{h,i}^k) \right\},$$
$$\tilde{X}_{h,0}^k = \left\{ v_h \in X_h^k : v_{h_{|\partial\Omega}} = 0 \right\},$$
$$\tilde{\mathbf{X}}_h^k = \tilde{X}_h^k \times \tilde{X}_h^k, \qquad \tilde{\mathbf{X}}_{h,0}^k = \tilde{X}_{h,0}^k \times \tilde{X}_{h,0}^k \quad \text{and}$$
$$\tilde{Y}_h^k = \left\{ q_h \in L^2(\Omega_h^k) : q_{h|K} \circ G_K^2 \in P_1(\hat{K}),\, q_{h|\Omega_{h,i}^k} \in C^0(\Omega_{h,i}^k) \right\}$$

and their *continuous* counterparts

$$X_h^k = \tilde{X}_h^k \cap C^0(\Omega_h^k), \qquad X_{h,0}^k = \tilde{X}_{h,0}^k \cap C^0(\Omega_h^k),$$
$$\mathbf{X}_h^k = X_h^k \times X_h^k, \qquad \mathbf{X}_{h,0}^k = X_{h,0}^k \times X_{h,0}^k \quad \text{and}$$
$$Y_h^k = \tilde{Y}_h^k \cap C^0(\Omega_h^k)$$

defined on the discretized domain Ω_h^k. The appropriate finite element pair for the unknowns $(\mathbf{u}^{k+1}, p^{k+1})$ is given by $\mathbf{X}_{h,0}^k \times \tilde{Y}_h^k$, i.e. globally continuous piecewise quadratic functions (on the reference element) for the velocity and piecewise linear functions (on the reference element) which are continuous in every subdomain $\Omega_{h,i}^k$, but may be discontinuous across Γ_h^k.

From an implementation point of view, it may be advantageous to work with the more general spaces $\tilde{\mathbf{X}}_h^k$, $\tilde{X}_h^k$ and $\tilde{Y}_h^k$ and use an additional projection step to enforce continuity for the velocity $\mathbf{u}^{k+1}$ on Γ_h^k. This strategy, denoted by SPM (Subspace Projection Method), was described in detail in [11] with respect to two-phase flows and in [10] with respect to particulate flows. Here, we only give a brief outline and consider again the generic discretized problem (24). Note that $\mathbf{X}_{h,0}^k$ is a vector subspace of the space $\tilde{\mathbf{X}}_h^k$. Therefore, we may define a projection

$$\mathcal{P} : \tilde{\mathbf{X}}_h^k \to \mathbf{X}_{h,0}^k. \tag{25}$$

In the discrete setting, the generic problem (24) reads: *Find* $(\mathbf{u}_h, \tilde{p}_h) \in \mathbf{X}_{h,0}^k \times \tilde{Y}_h^k$ *such that*

$$s\left((\mathbf{u}_h, \tilde{p}_h), (\mathbf{v}_h, \tilde{q}_h)\right) = g(\mathbf{v}_h, \tilde{q}_h) \quad \text{for all } (\mathbf{v}_h, \tilde{q}_h) \in \mathbf{X}_{h,0}^k \times \tilde{Y}_h^k. \tag{26}$$

Equivalently, one may rewrite problem (26) using the projection operator (25) as: *Find* $(\tilde{\mathbf{u}}_h, \tilde{p}_h) \in \tilde{\mathbf{X}}_h^k \times \tilde{Y}_h^k$ *such that*

$$s\left((\mathcal{P}\tilde{\mathbf{u}}_h, \tilde{p}_h), (\mathcal{P}\tilde{\mathbf{v}}_h, \tilde{q}_h)\right) = g(\mathcal{P}\tilde{\mathbf{v}}_h, \tilde{q}_h) \quad \text{for all } (\tilde{\mathbf{v}}_h, \tilde{q}_h) \in \tilde{\mathbf{X}}_h^k \times \tilde{Y}_h^k \tag{27}$$

and set $\mathbf{u}_h = \mathcal{P}\tilde{\mathbf{u}}_h$.

If we denote by $\boldsymbol{\varphi}_i$ the basis functions of $\tilde{\mathbf{X}}_h$ and by ψ_i the basis functions of $\tilde{Y}_h$, elements $\tilde{\mathbf{u}}_h \in \tilde{\mathbf{X}}_h^k$ and $\tilde{p}_h \in \tilde{Y}_h^k$ can be represented uniquely by the nodal vectors $\underline{\tilde{\mathbf{u}}} \in \mathbb{R}^{2N}$ and $\underline{\tilde{p}} \in \mathbb{R}^M$, i.e.

$$\tilde{\mathbf{u}}_h(\mathbf{x}) = \sum_{i=1}^{2N} \underline{\tilde{\mathbf{u}}}_i \boldsymbol{\varphi}_i(\mathbf{x}) \quad \text{and} \quad \tilde{p}_h(\mathbf{x}) = \sum_{i=1}^{M} \underline{\tilde{p}}_i \psi_i(\mathbf{x}).$$

If we denote by $\hat{P}$ the discrete version of the projection $\mathcal{P}$ acting on the nodal vector $\underline{\tilde{\mathbf{u}}}_i$,

$$P\begin{bmatrix}\underline{\tilde{\mathbf{u}}}\\ \underline{\tilde{p}}\end{bmatrix} = \begin{bmatrix}\hat{P}\underline{\tilde{\mathbf{u}}}\\ \underline{\tilde{p}}\end{bmatrix} \quad \text{and} \quad P^T\begin{bmatrix}\underline{\tilde{\mathbf{u}}}\\ \underline{\tilde{p}}\end{bmatrix} = \begin{bmatrix}\hat{P}^T\underline{\tilde{\mathbf{u}}}\\ \underline{\tilde{p}}\end{bmatrix}$$

defines the combined projection P and its adjoint mapping P^T. Let us denote by S the system matrix arising from the discretization of $s : (\tilde{X}_h^k \times \tilde{Y}_h^k) \times (\tilde{X}_h^k \times \tilde{Y}_h^k)$ and by G the corresponding discretized right hand side. The resulting linear system for problem (27) then reads:

Find $[\underline{\tilde{\mathbf{u}}}, \underline{\tilde{p}}]^T \in \mathbb{R}^{2N+M}$ *such that*

$$P^T S P \begin{bmatrix}\underline{\tilde{\mathbf{u}}}\\ \underline{\tilde{p}}\end{bmatrix} = P^T G \tag{28}$$

and set $\underline{\mathbf{u}} = \hat{P}\underline{\tilde{\mathbf{u}}}$.

In a numerical realization, the system matrix $P^T S P$ does not have to be assembled explicitly. Instead, if iterative solvers are used to solve the systems, simple routines can perform the action of the discrete operators P and P^T on vectors, see [11] for more details.

Let us introduce the following matrices arising from the discretization of the forms (18):

$$\begin{aligned}
&M_{i,j}^k = m(\Omega_h^k; \boldsymbol{\varphi}_j, \boldsymbol{\varphi}_i), \qquad A_{i,j}^k = a(\Omega_h^k; \boldsymbol{\varphi}_j, \boldsymbol{\varphi}_i),\\
&C^k(\mathbf{v})_{i,j} = c(\Omega_h^k; \mathbf{v}; \boldsymbol{\varphi}_j, \boldsymbol{\varphi}_i), \qquad D_{i,j}^k = d(\Omega_h^k; \boldsymbol{\varphi}_j, \boldsymbol{\varphi}_i) \quad \text{and}\\
&B_{j,l}^k = b(\Omega_h^k; \psi_l, \boldsymbol{\varphi}_i)
\end{aligned} \tag{29}$$

and

$$\underline{f}_i^k = f(\Omega_h^k; \boldsymbol{\varphi}_i), \qquad \underline{e}_i^k = e(\Gamma_h^k; \boldsymbol{\varphi}_i). \tag{30}$$

Applying the subspace projection method (28) to the time discrete problems (21) and (22) yields the following fully discrete scheme (we omit the third substep (23) which reads as the first one with obvious modifications):

(dQS1): *Find* $\underline{\mathbf{u}}^{k+\Theta}, \underline{\tilde{p}}^{k+\Theta} \in \mathbb{R}^{2N} \times \mathbb{R}^M$ *such that*

$$\begin{aligned}
&\hat{P}^T V_{Q1} \hat{P} \underline{\tilde{\mathbf{u}}}^{k+\Theta} + \Theta\tau \hat{P}^T B^k \underline{\tilde{p}}^{k+\Theta} = \hat{P}^T \underline{f}_{Q1},\\
&(B^k)^T \hat{P} \underline{\tilde{\mathbf{u}}}^{k+\Theta} = 0\\
&\text{with } \underline{f}_{Q1} = M^k \underline{\mathbf{u}}^k + \Theta\tau\left(-\beta A^k \underline{\mathbf{u}}^k - C^k(\underline{\mathbf{u}}^k - \underline{\mathbf{w}}^k)\underline{\mathbf{u}}^k + \underline{f}^{k+\Theta} - \underline{e}^k\right),\\
&V_{Q1} = M^k + \Theta\tau\left(\alpha A^k + \tau D^k\right) \quad \text{and}\\
&\underline{\mathbf{u}}^{k+\Theta} = \hat{P}\underline{\tilde{\mathbf{u}}}^{k+\Theta}.
\end{aligned} \tag{31}$$

(dNL): *Find* $\underline{\mathbf{u}}^{k+\Theta'} \in \mathbb{R}^{2N}$ *such that*

$$\begin{aligned}
&\hat{P}^T V_N(\underline{\mathbf{u}}^{k+\Theta'})\hat{P}\tilde{\underline{\mathbf{u}}}^{k+1} = \hat{P}^T \underline{f}_N \\
&\text{with } \underline{f}_N = M^k \underline{\mathbf{u}}^{k+\Theta} + (1-2\Theta)\tau\left(-\alpha A^k \underline{\mathbf{u}}^{k+\Theta'} + \underline{f}^{k+\Theta'} - \underline{e}^k - B^k \underline{\tilde{p}}^{k+\Theta}\right), \\
&V_N = M^k + (1-2\Theta)\tau\left(\beta A^k + C^k(\underline{\mathbf{u}}^{k+\Theta'} - \underline{\mathbf{w}}^k) + \tau D^k\right) \quad \text{and} \\
&\underline{\mathbf{u}}^{k+\Theta'} = \hat{P}\tilde{\underline{\mathbf{u}}}^{k+\Theta'}.
\end{aligned} \tag{32}$$

4.5. Discretization of the level set equation

For the level set Eq. (8), we employ streamline diffusion stabilized P_2 finite elements for space discretization and an implicit Euler time discretization. Since in our code the discontinuous space $\tilde{X}_h^k$ is implemented, we again use the subspace projection method to enforce continuity of ϕ across Γ. Consider the nodal vector $\underline{\tilde{\phi}}^{k+1} \in \mathbb{R}^N$ representing the discontinuous function $\tilde{\phi}_h^{k+1} \in \tilde{X}_h^k$ by

$$\tilde{\phi}_h^{k+1}(\mathbf{x}) = \sum_{i=1}^{N} \underline{\tilde{\phi}}_i^{k+1} \varphi_i(\mathbf{x}),$$

where φ_i are the N basis functions of $\tilde{X}_h^k$. The stabilized mass matrix $M(\mathbf{v}) \in \mathbb{R}^{N\times N}$ and the stabilized convection matrix $K(\mathbf{v}) \in \mathbb{R}^{N\times N}$ are defined by

$$\begin{aligned}
M_{i,j}(\mathbf{v}) &= \int_{\Omega_h^k} \varphi_j(\varphi_i + \delta\mathbf{v}\cdot\nabla\varphi_i) \quad \text{and} \\
K_{i,j}(\mathbf{v}) &= \int_{\Omega_h^k} \mathbf{v}\cdot\nabla\varphi_j(\varphi_i + \delta\mathbf{v}\cdot\nabla\varphi_i) \quad \forall i,j \in \{1,\dots,N\},
\end{aligned}$$

where $\delta \geq 0$ denotes the streamline diffusion parameter. The linear system of equations for the (discontinuous) level set FE vector $\underline{\tilde{\phi}}^{k+1} \in \mathbb{R}^{k+1}$ then reads:

$$\hat{P}^T\left(M(\mathbf{u}^{k+1} - \mathbf{w}^k) + \tau K(\mathbf{u}^{k+1} - \mathbf{w}^k)\right)\hat{P}\underline{\tilde{\phi}}^{k+1} = \hat{P}^T M(\mathbf{u}^{k+1} - \mathbf{w}^k)\underline{\phi}^k. \tag{33}$$

The finite element vector representing the continuous level set function is again obtained by

$$\underline{\phi}^{k+1} = \hat{P}\underline{\tilde{\phi}}^{k+1}.$$

During the time stepping procedure, the level set function might degenerate in such a way that the mesh optimization would fail. This is mainly due to spurious oscillations which occur in the vicinity of Γ. In order to "repair" the level set function, we periodically perform a redistancing step. Note that since in our method the interface is always known explicitly in terms of Γ_h, no additional explicit reconstruction of the interface has to be performed. Consequently, efficient redistancing algorithms exploiting this fact can be designed, see for instance [7].

5. Numerical results

In [7], we have already reported on numerical results of our method applied to a stationary problem and a two-phase flow benchmark problem. In this section, we present two additional examples which demonstrate the benefits but also limitations of our method. At this point we would also like to recall that due to our aligned mesh strategy which accurately allows us to capture pressure jumps at the interface and the variational treatment of the curvature, spurious velocities close to the interface are almost absent. This also makes frequent redistancing for the level set function unnecessary.

5.1. Oscillating droplet

In this first example, we consider the behavior of an oscillating droplet which is a well-studied problem. In particular, analytical results concerning the droplet's shape, amplitude and frequency of oscillation exist [25]. Results of our method were already reported in [12] and we only give a brief summary.

Consider a spherical droplet of radius r_0 in its unperturbed state. Let $\varepsilon > 0$ denote the amplitude and $n > 0$ the mode of oscillation. The surface of the drop in polar coordinates is given by

$$(r,\theta) = (r_0 + \varepsilon\cos(n\theta),\theta) \quad \text{for } \theta \in [0, 2\pi). \tag{34}$$

For the oscillation frequency $\tilde{\omega}_n$ of the drop

$$\tilde{\omega}_n^2 = \frac{n^3 - n}{\tilde{r}_0^3}\frac{\sigma}{\rho_1 + \rho_2}$$

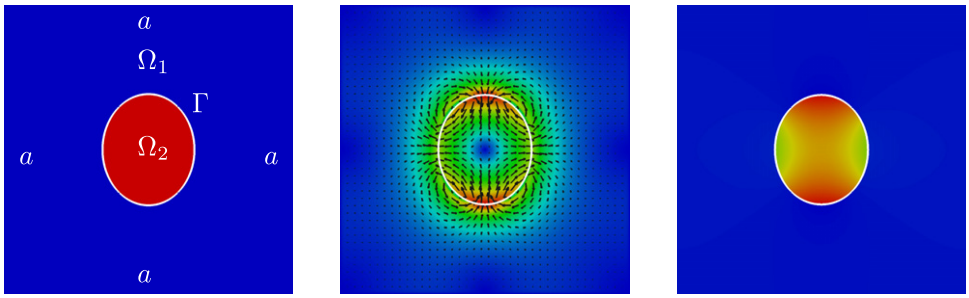

Fig. 2. Oscillating bubble: Initial configuration (left), velocity profile (middle) and pressure profile (right) at $t = 0.01$.

Table 1
Estimated frequency, damping parameter and volume of the discrete droplet at the final time instant.

Quantity	$l = 4$	$l = 5$	$l = 6$	Exact
ω_2	50.24	49.86	49.74	50.4420
γ	1.94	1.89	1.84	–
$V(t_{N_k})$	0.3804	0.3828	0.3837	0.3848

holds, where ρ_i is the density of the fluid in subdomain Ω_i and σ denotes the surface tension coefficient in (2). The physical parameters for the simulation are chosen as:

$$\rho_1 = 0.1\,\frac{\text{kg}}{(\text{dm})^3}, \qquad \rho_2 = 1\,\frac{\text{kg}}{(\text{dm})^3}, \qquad \sigma = 50\cdot 10^{-3}\,\frac{\text{N}}{\text{m}},$$
$$\mu_1 = 0.1\cdot 10^{-3}\ \text{Pa s}, \qquad \mu_2 = 0.4\cdot 10^{-3}\ \text{Pa s}, \qquad \tilde{r}_0 = 0.35\cdot 10^{-3}\ \text{m}.$$

The characteristic quantities are $L = 10^{-3}$ m, $U = 50\cdot 10^{-3}\,\frac{\text{m}}{\text{s}}$ and $\rho_c = 0.5(\rho_1+\rho_2)$ such that we end up with the following dimensionless quantities,

$$\Lambda_1 = \frac{2}{11}, \qquad \Lambda_2 = \frac{20}{11}, \qquad \text{Re}_1 = 275, \qquad \text{Re}_2 = 68.75, \qquad \text{We} = 0.0275,$$

a frequency $\omega_2 = 50.4420$ and a periodic time $T_p = \frac{2\pi}{\omega_2} = 0.124563$ for the second mode.

In our computations, we consider a domain $\Omega = (-1, 1)^2$ and time interval $I = [0, 2]$. The initial shape of the droplet is given by (34) with $\varepsilon = 0.1$, and we prescribe homogeneous Dirichlet boundary conditions at the walls, see Fig. 2. We discretize Ω using uniform triangulations of edge length $h_l = 2^{3/2}\cdot 2^{-l}$ for $l = 4, 5, 6$ and use a fixed time step size of $\tau = 2\cdot 10^{-3}$. During the simulation, we track the height $\bar{h}(t)$ of the droplet over time and consider its deflection d from the unperturbed radius r_0: $d(t) = 0.5\bar{h}(t) - r_0$. $d(t)$ is a damped oscillation and can be described by a function

$$d_f(t) = d_f(t; a_0, p_0, \gamma, \omega) = a_0\exp(-\gamma t)\cos(t\omega + p_0), \tag{35}$$

where a_0 is the initial amplitude, p_0 the phase, γ denotes the damping parameter and ω denotes the frequency. For each refinement level l, we perform a least square fit, i.e. we minimize

$$\sum_{k=1}^{N_k} \|d_f(t_k) - d(t_k)\|^2$$

to obtain the parameters. We also compute the volume of the discrete droplet at the final time instant and denote it by $V(t_{N_k})$. Results are shown in Table 1. Concerning the frequency, we see good accordance with the theoretical estimate (50.442) on all refinement levels. We also observe that although no volume correction or redistancing step for the level set function was performed, the relative error of $V(t_{N_k})$ after 1000 time steps is less than 1.2% on the coarsest level ($l = 4$) and less than 0.5% on the finest level ($l = 6$).

5.2. Two-phase flow benchmark problem

Results of our method applied to the well-known two-phase flow benchmark problem by Hysing et al. [26] were already reported in [7] for the "mild" parameter set. In this paper we also present results for the "challenging" parameter set.

The initial geometry of the benchmark problem is sketched in Fig. 3 and we refer the reader to [26] for a more detailed description of the setting. The physical parameters in this benchmark lead to the following two sets of dimensionless numbers (Table 2): The quantities of interest in this benchmark problem are

1. Volume $\tilde{V}(t) = \int_{\Omega_2(t)} 1 d\mathbf{x}$.

Table 2
Dimensionless parameters for the "mild" and "challenging" parameters of the two-phase flow benchmark problem.

Case	Λ_1	Λ_2	Re_1	Re_2	We
"Mild"	10	1	3.5	35	1
"Challenging"	10	0.01	3.5	350	12.5

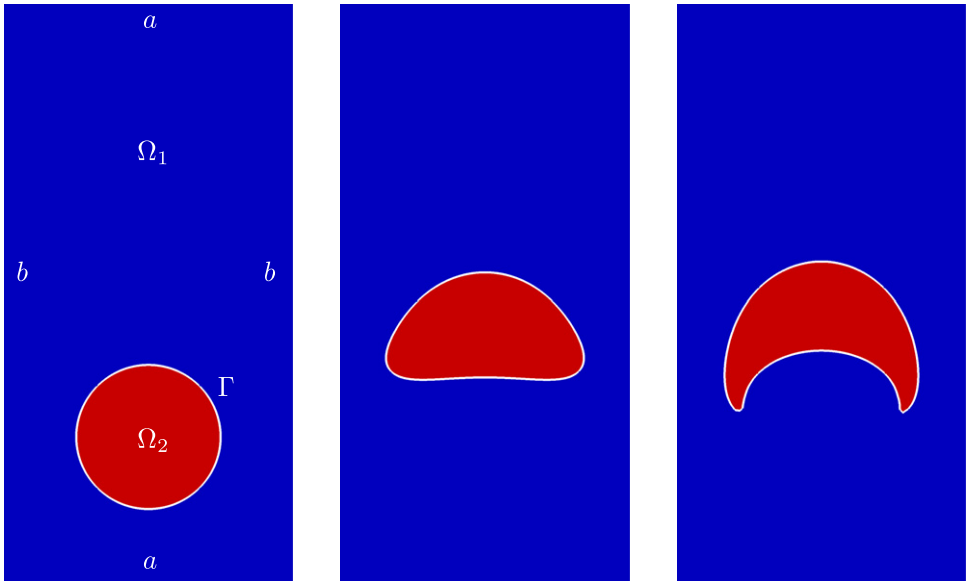

Fig. 3. Rising bubble benchmark: Initial configuration (left), bubble shape at $t = 1.86$ for the "mild" parameter set (middle) and the "challenging" parameter set (right).

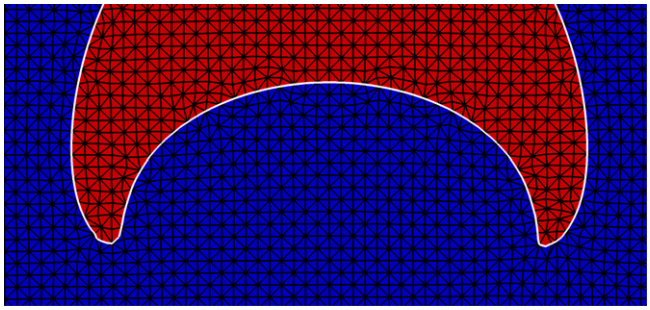

Fig. 4. Triangulation of the domain shortly before simulation breakdown.

2. Circularity $\not{c}(t) = \frac{\text{perimeter of area-equivalent circle}}{\text{perimeter of bubble}}$, measuring the deviation of the droplets' shape from a circle.
3. Average rise velocity $U(t) = \frac{\int_{\Omega_2(t)} \mathbf{u}^{(1)} dx}{V(t)}$.

As in the previous problem, we discretize Ω using uniform triangulations corresponding to refinement levels $l = 5, 6$. This corresponds to a mesh consisting of 4096 elements ($l = 5$) and 16 384 ($l = 6$) elements, respectively. We choose a constant time step size $\tau = 5 \cdot 10^{-3}$. In Fig. 3, we depict the shape of the bubble at time instant $t = 1.86$ for the "mild" and the "challenging" parameter set. While for the "mild" case we were able to conduct the full benchmark problem until the final time instant $t = 3$, the simulation breaks down in the "challenging" case due to the complexity of the geometry. Since we use uniform meshes without h-adaptivity, the mesh optimization breaks down once the simulation approaches the point when the interface shape becomes too complex (at approximately $t = 1.5$ on $l = 5$ and $t = 1.86$ on $l = 6$) to be resolved by the mesh. The triangulation for $l = 6$ shortly before the breakdown is depicted in Fig. 4.

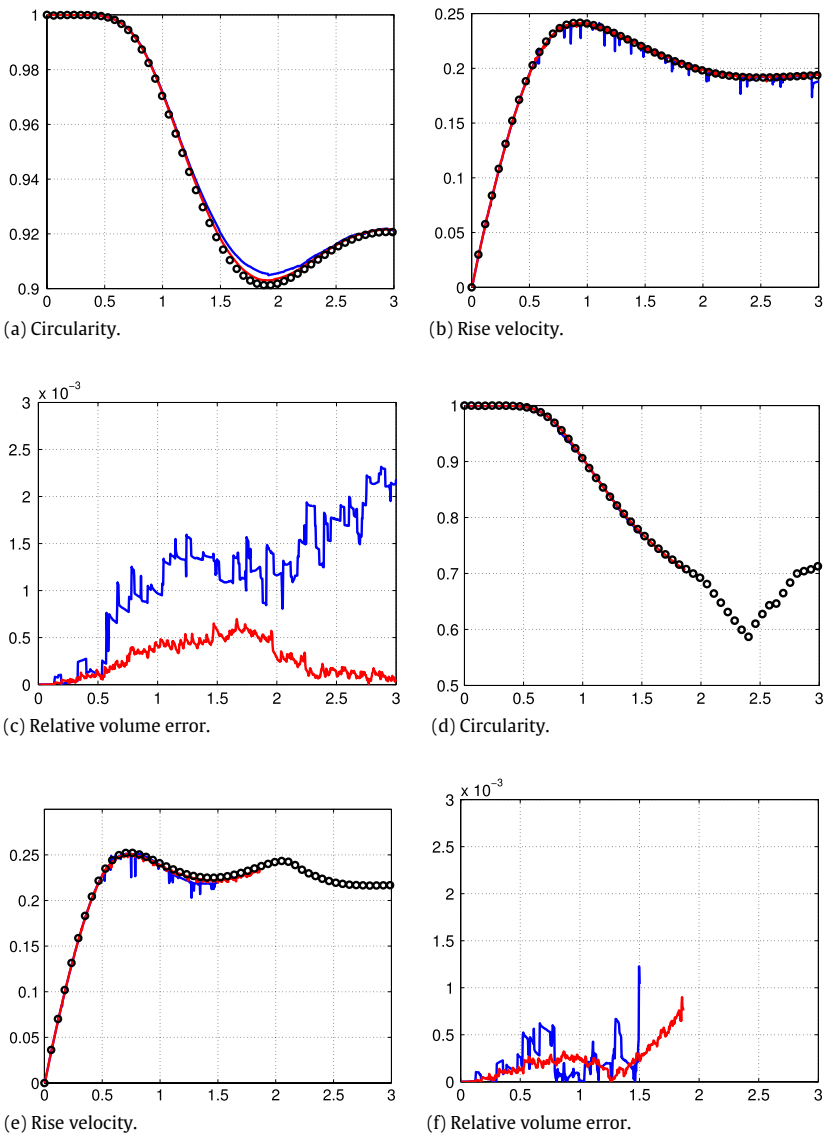

Fig. 5. Time evolution of the benchmark quantities. (a)–(c): "Mild" parameter set, (d)–(f): "challenging" parameter set. Results on refinement level $l = 5$ are represented by blue lines, on $l = 6$ by red lines. Black circles correspond to reference values. (For interpretation of the references to colour in this figure legend, the reader is referred to the web version of this article.)

In Fig. 5, we depict the results of our approach for both the "mild" and the "challenging" case up to the end of the simulation (or breakdown in the "challenging" setting). We also add the reference solution obtained by the flow solver TP2D [27].

Note that in both cases, we obtain good agreement for all considered quantities despite the relative coarse space discretization. We also note that although we do not use any volume correction for the level set function, the relative error in volume is less than 0.25% in all simulations.

6. Conclusion

We presented details on the numerical realization of a new finite element method for two-phase flow simulations which was recently introduced in [7]. The main ingredient is a hybrid representation of the interface between the fluid phases which is provided implicitly by a level set function and explicitly by an aligned mesh obtained using a black-box optimization approach.

Space discretization is based on quadratic Taylor–Hood finite elements for the Navier–Stokes equations and quadratic finite elements for the level set equation defined on isoparametric elements. The mesh alignment allows us to accurately treat discontinuities of the solution (pressure) across the interface and, together with a variational approach for the curvature

of the interface, surface tension can be approximated very precisely. The discontinuity of the finite element space for the pressure is realized using a subspace projection method (SPM).

Our time discretization is based on an explicit decoupling of the Navier–Stokes and level set equations. While the Navier–Stokes equations are treated using a fractional step theta-scheme, the level set equation is treated using an implicit Euler scheme. Equations are formulated in arbitrary Lagrangian–Eulerian (ALE) coordinates which makes remeshing unnecessary.

We presented two numerical experiments for which reference solutions are available and evaluated the benefits but also the limitations of the proposed method. These limitations are mainly due to us using uniform meshes without local adaptivity. Combining the proposed approach with local adaptivity will be subject of further work.

References

[1] S. Osher, J.A. Sethian, Fronts propagating with curvature-dependent speed: algorithms based on Hamilton–Jacobi formulations, J. Comput. Phys. 79 (1) (1988) 12–49.
[2] S. Osher, R. Fedkiw, Level Set Methods and Dynamic Implicit Surfaces, Springer Verlag, 2003.
[3] C.W. Hirt, B.D. Nichols, Volume of fluid (VOF) method for the dynamics of free boundaries, J. Comput. Phys. 39 (1) (1981) 201–225.
[4] T.J.R. Hughes, W. Liu, T.K. Zimmermann, Lagrangian–Eulerian finite element formulation for incompressible viscous flows, Comput. Methods Appl. Mech. Eng. 29 (3) (1981) 329–349.
[5] T. Tezduyar, R. Benney, Mesh moving techniques for fluid–structure interactions with large displacements, J. Appl. Mech. (2003).
[6] Thomas Wick, Fluid–structure interactions using different mesh motion techniques, Comput. Struct. 89 (1314) (2011) 1456–1467.
[7] Steffen Basting, Martin Weismann, A hybrid level setfront tracking finite element approach for fluidstructure interaction and two-phase flow applications, J. Comput. Phys. 255 (0) (2013) 228–244.
[8] Steffen Basting, Rodolphe Prignitz, An interface-fitted subspace projection method for finite element simulations of particulate flows, Comput. Methods Appl. Mech. Eng. 267 (0) (2013) 133–149.
[9] R. Prignitz, E. Bänsch, Numerical simulation of suspension induced rheology, Kybernetika 46 (2) (2010) 281–293.
[10] R. Prignitz, E. Bänsch, Particulate flows with the subspace projection method, Department Mathematik, Universität Erlangen–Nürnberg, 2012, Preprint 360. http://www.math.fau.de/fileadmin/preprints/pr360.pdf.
[11] Kathrin Bäumler, Eberhard Bänsch, A subspace projection method for the implementation of interface conditions in a single-drop flow problem, J. Comput. Phys. 252 (0) (2013) 438–457.
[12] Martin Weismann, The hybrid level-set front-tracking approach, Master's Thesis, Friedrich-Alexander University Erlangen–Nuremberg, 2012.
[13] M. Rumpf, A variational approach to optimal meshes, Numer. Math. 72 (1996) 523–540.
[14] B. Bejanov, J.L. Guermond, P.D. Minev, A grid-alignment finite element technique for incompressible multicomponent flows, J. Comput. Phys. 227 (13) (2008) 6473–6489.
[15] G. Dziuk, An algorithm for evolutionary surfaces, Numer. Math. 58 (1) (1990) 603–611.
[16] J.U. Brackbill, D.B. Kothe, C. Zemach, A continuum method for modeling surface tension, J. Comput. Phys. 100 (2) (1992) 335–354.
[17] E. Bänsch, Finite element discretization of the Navier–Stokes equations with a free capillay surface, Numer. Math. 88 (2) (2001) 203–235.
[18] M.O. Bristeau, R. Glowinski, J. Periaux, Numerical methods for the Navier–Stokes equations. Applications to the simulation of compressible and incompressible viscous flows, Comput. Phys. Rep. 6 (16) (1987) 73–187.
[19] Luca Formaggia, Fabio Nobile, A stability analysis for the arbitrary Lagrangian Eulerian formulation with finite elements, East West J. Numer. Math. 7 (1999) 105–132.
[20] Luca Formaggia, Fabio Nobile, Stability analysis of second-order time accurate schemes for alefem, Comput. Methods Appl. Mech. Eng. 193 (3941) (2004) 4097–4116. The Arbitrary Lagrangian–Eulerian Formulation.
[21] Burkhard Höhn, Numerik für die Marangoni-Konvektion beim Floating-Zone Verfahren, Ph.D. Thesis, Universitätsbibliothek Freiburg, 1999.
[22] S. Ganesan, G. Matthies, L. Tobiska, On spurious velocities in incompressible flow problems with interfaces, Comput. Methods Appl. Mech. Eng. 196 (7) (2007) 1193–1202.
[23] S. Groß, A. Reusken, An extended pressure finite element space for two-phase incompressible flows with surface tension, J. Comput. Phys. 224 (1) (2007) 40–58.
[24] S. Zahedi, M. Kronbichler, G. Kreiss, Spurious currents in finite element based level set methods for two-phase flow, Internat. J. Numer. Methods Fluids 69 (9) (2012) 1433–1456.
[25] D.E. Fyfe, E.S. Oran, M.J. Fritts, Surface tension and viscosity with Lagrangian hydrodynamics on a triangular mesh, J. Comput. Phys. 76 (2) (1988) 349–384.
[26] S. Hysing, S. Turek, D. Kuzmin, N. Parolini, E. Burman, S. Ganesan, L. Tobiska, Quantitative benchmark computations of two-dimensional bubble dynamics, Internat. J. Numer. Methods Fluids 60 (11) (2009) 1259–1288.
[27] S. Turek, Efficient Solvers for Incompressible Flow Problems: An Algorithmic and Computational Approach, Springer, ISBN: 3-540-65433-X, 1999.